

nism requires a much smaller sweep volume for isomerization than the rotation mechanism, so that the azobenzene derivatives undergo isomerization in relatively rigid matrices such as polymer matrices below  $T_g$ , depending on the spatial and temporal distribution of the free volume in the polymer (13–15). Below  $T_g$ , segmental movement of the main chain of the polymers is frozen; however, movement of side chains is allowed to some extent.

In a system in which the center of gravity of each molecule is aligned regularly, as in crystals, optical anisotropy still remains active even after the anisotropy in the shape of each molecule vanishes (Fig. 6A). On the other hand, in NLCs optical anisotropy arises only from the anisotropy in the molecular shape (rod-like shape); the center of gravity of each molecule is random. Therefore, in the NLCs the optical anisotropy disappears if the anisotropy in the shape of each molecule is eliminated by trans-cis isomerization (Fig. 6B). This behavior provides the basis of the microsecond response time observed for the polymeric NLC film in the present study.

## Observation of Shoemaker-Levy Impacts by the Galileo Photopolarimeter Radiometer

Terry Z. Martin,\* Glenn S. Orton, Larry D. Travis, Leslie K. Tamppari, Ian Claypool

The Galileo Photopolarimeter Radiometer experiment made direct photometric observations at 678 and 945 nanometers of several comet Shoemaker-Levy 9 fragments impacting with Jupiter. Initial flashes occurred at (fragment G) 18 July 1994 07:33:32, (H) 18 July 19:31:58, (L) 19 July 22:16:48, and (Q1) 20 July 20:13:52 [equivalent universal time coordinated (UTC) observed at Earth], with relative peak 945-nanometer brightnesses of 0.87, 0.67, 1.00, and 0.42, respectively. The light curves show a 2-second rise to maximum, a 10-second plateau, and an accelerating falloff. The Q1 event, observed at both wavelengths, yielded a color temperature of more than 10,000 kelvin at its peak.

The impact of comet Shoemaker-Levy 9 (SL9) into Jupiter in July 1994 stimulated an unparalleled set of astronomical observations. The instrument complement of the Galileo spacecraft, on its way to a December 1995 orbit insertion at Jupiter, observed the impact events directly from a vantage point above the dawn terminator. A number of Earth-based observers have reported detection of impact-related phenomena at times preceding those from Galileo, in spite of the impacts occurring behind the limb of

## REFERENCES AND NOTES

1. K. Ogura, H. Hirabayashi, A. Uejima, K. Nakamura, *Jpn. J. Appl. Phys.* **21**, 969 (1982).
2. S. G. Odulov, Yu. A. Reznikov, M. S. Soskin, A. I. Khizhnyak, *Sov. Phys. JETP* **58**, 1154 (1983).
3. M. Eich and J. H. Wendorff, *Makromol. Chem. Rapid Commun.* **8**, 467 (1987).
4. K. Anderle, R. Birenheide, M. Eich, J. H. Wendorff, *ibid.* **10**, 477 (1989).
5. S. Kurihara, T. Ikeda, T. Sasaki, H.-B. Kim, S. Tazuke, *J. Chem. Soc. Chem. Commun.* **1990**, 1751 (1990).
6. T. Ikeda, T. Sasaki, H.-B. Kim, *J. Phys. Chem.* **95**, 509 (1991).
7. S. Kurihara, T. Ikeda, S. Tazuke, J. Seto, *J. Chem. Soc. Faraday Trans.* **87**, 3251 (1991).
8. T. Ikeda, T. Sasaki, K. Ichimura, *Nature* **361**, 428 (1993).
9. K. Ichimura, Y. Hayashi, H. Akiyama, N. Ishizuki, *Langmuir* **9**, 3298 (1993).
10. A. S. Angeloni, D. Caretti, C. Carlini, G. Chiellini, G. Galli, *Liq. Crystals* **4**, 513 (1989).
11. H. Rau and E. J. Luddecke, *J. Am. Chem. Soc.* **104**, 1616 (1982).
12. T. Naito, K. Horie, I. Mita, *Macromolecules* **24**, 2907 (1991).
13. C. S. P. Sung, I. R. Gould, N. J. Turro, *ibid.* **17**, 1447 (1984).
14. J. G. Victor and J. M. Torkelson, *ibid.* **20**, 2241 (1987).
15. I. Mita, K. Horie, K. Hirao, *ibid.* **22**, 558 (1989).

3 February 1995; accepted 27 April 1995

Jupiter as viewed from Earth. Correlation of these disparate data sets should lead to a model of how those singular events took place. We report here observations by the Photopolarimeter Radiometer (PPR) (1), a single-field-of-view instrument that uses a rotating filter wheel covering wavelengths in the visible and near infrared for photometric and polarimetric remote sensing of Jupiter's atmosphere and satellites.

For the SL9 observations, the PPR was used as a high-speed photometer, maximizing the likelihood of observing the radiation associated with the impact events, given the considerable uncertainty about their magnitude, timing, and duration (2). Consequently, single-filter measurements with a 0.23-s sample time were used for most of the observed impacts.

Among the available wavelengths, we selected 678 and 945 nm (with bandwidths of 9 and 11 nm, respectively). Most events were observed at 945 nm alone, to allow detection of thermal emission from a rapidly rising fireball, which at some 3000 K (3, 4) would be cooler than the entry meteor flash. For fragment Q1, however, measurements alternated between 678 and 945 nm, with a sample period of 1.26 s at either wavelength.

For impact events B, H, L, Q1, and S, the PPR 2.5-mrad field of view was centered on Jupiter's 0.6-mrad disk (5), and the data were buffered in the spacecraft computer memory and read out within 1 day (6). For the C, G, and R events, the PPR was set up to record data on tape simultaneously with the infrared and ultraviolet spectrometer measurements (7).

Detection of an impact event by the PPR depended on (i) the time of the actual impact relative to a fixed observing interval, defined in mid-June, (ii) the brightness of the impact, and (iii) the amount of stored data that could be returned within the available downlink communication time. Among the set of memory-buffered observations, definite signals were found for H, L, and Q1 (8) (Figs. 1 and 2). These events were all much shorter than the observed time span (Table 1). The  $1\sigma$  noise level at 945 nm for all observations was 1.2 data numbers (DN) after averaging the two polarization channel signals together without smoothing (2). This is about 0.5% of the integrated brightness of Jupiter at 945 nm.

All of the events detected rose to maximum signal within 2 s, at which time there was a sudden slope change at the peak intensity. All of the 945-nm measurements had a similar shape, with about a 10-s plateau before falloff. The maximum duration of detected light was 35 s for the impact of fragment L. Data returned from the G impact, although sampled less frequently, show the same general behavior as the others (Fig. 3). There was a suggestion of secondary flashes in the 3 min following the main G flash. However, examination of the two PPR channels shows a lack of correlated signals during this period, and it is unlikely that these peaks are real. It should be pointed out that there is no structure in the G, H, or L data indicating the detection of separate meteor and fireball phases, except perhaps for the slope change.

The 678-nm signal for Q1 decayed faster (Fig. 4) (9). The brightness curve extracted from the time-drift images of impact K at 890 nm by the Solid State Imaging (SSI) instrument on Galileo (10) shows a similar shape and a duration comparable to our 945-nm data for G, H, and L. The SSI sequence of images for impact W at 559 nm show a rise and fall within about 5 s, which is similar

T. Z. Martin, G. S. Orton, L. K. Tamppari, I. Claypool, Jet Propulsion Laboratory, 4800 Oak Grove Drive, MS 169-237, California Institute of Technology, Pasadena, CA 91109, USA.

L. D. Travis, Goddard Institute for Space Studies, 2880 Broadway, New York, NY 10025, USA.

\*To whom correspondence should be addressed.

to the behavior seen for Q1 at 678 nm.

The PPR flashes could represent (i) the hot meteor phase of the fragment's demise, with a duration indicative of the time for the glowing trail material to radiate its energy, (ii) the meteor phase during the rising

part of the curve, followed by the "fireball" phase, the explosive expansion of hot material after the meteor deposited its energy, or (iii) only the fireball phase. Clues to the origin of the light seen by the PPR can be found in the absolute intensities, in the

ratio of intensities at different wavelengths, and in the correlation with other data sets.

The peak absolute signal levels observed by the PPR at 945 nm represent about 6% of the signal from Jupiter itself for the L event. The signal can be modeled by

$$S_{945} = B_{945}(T(t))\omega(t) \quad (1)$$

where  $T(t)$  is the temperature as a function of time  $t$ ,  $B(T(t))$  is the time-dependent Planck function, and  $\omega(t)$  is the effective solid angle subtended by the emission. The angular size and temperature-driven brightness cannot both be determined uniquely from the peak signal. For example, a 10,000-K meteor with a cross-sectional area of 150 km<sup>2</sup> (which could be a "pencil" of 2.5 km by 60 km) or a 3000 K fireball of 400 km<sup>2</sup> are equally consistent with the data.

A substantial clue to the interpretation is provided by the 678-nm flux to 945-nm flux ratio for Q1. At the peak, the ratio indicates a color temperature of 18,000 K, if blackbody emission is assumed (Fig. 4) (11). At 18,000 K, a source area of ~5 km<sup>2</sup> is adequate. The high emission at 678 nm relative to that at 945 nm implies that a hot and compact source was responsible for the earliest few seconds of the PPR light curve. The sharp drop-off of radiation at 678 nm

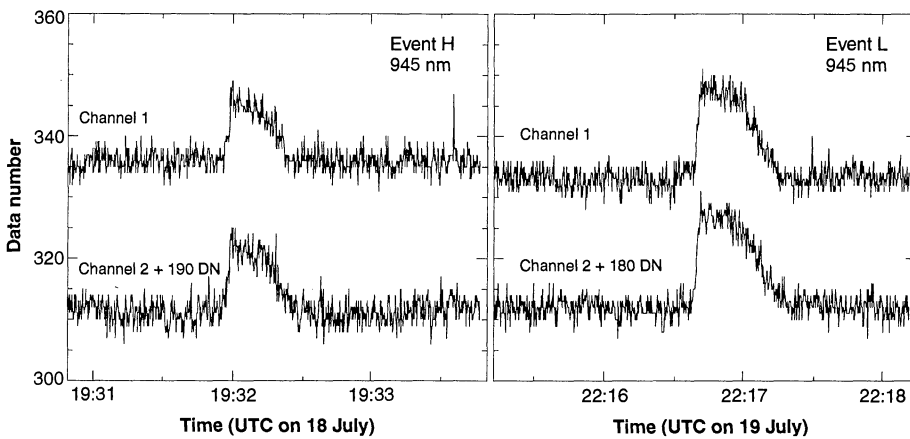


**Fig. 1.** Fragment H and L impacts. Raw signal traces for the two orthogonal polarization channels of the PPR. Differences in the ambient level of the two channels are the result of electronic drift of the zero-radiance level; the dark current restoration procedure normally performed was omitted here to avoid filter wheel stepping and consequent loss of time resolution. Offsets have been applied to channel 2 data to facilitate comparison. Sample interval is 0.23 s.

**Fig. 2.** Fragment Q1 impact. Raw signal traces for the two orthogonal polarization channels of the PPR for both the 678- and 945-nm filters, which were viewed alternately. Differences in the ambient level of the two polarization channels are the result of electronic drift; offsets have been applied to facilitate comparison. Sample interval is 1.26 s for a given filter.

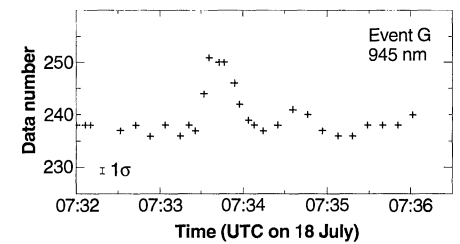
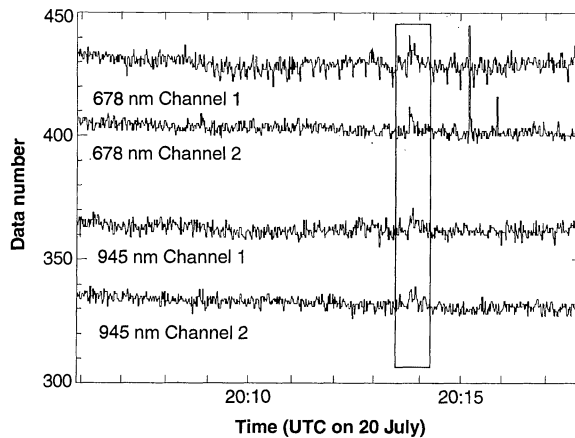


**Fig. 3.** Fragment G impact. Peak signal levels obtained during the repetitive scanning motion across Jupiter, with a period of 5.3 s. The average of the two orthogonal polarization channels of the PPR is shown.

**Table 1.** Galileo PPR observations.

Fragment	Date	Initial flash time*	Observation time span†	Wavelength (nm)	Signal maximum‡ (W cm <sup>-2</sup> nm <sup>-1</sup> )	Sample interval (s)	Note
B	17 July	Not seen	02:22:12–03:03:00	945	—	0.23	Signal too weak to be seen.
C	17 July	Not seen			—	5.3	Recorded, but not played back.
G	18 July	07:33:32	07:32:00–07:40:00	945	$2.1 \times 10^{-15}$	5.3	
H	18 July	19:31:58	19:11:24–19:52:12	945	$1.8 \times 10^{-15}$	0.23	
L	19 July	22:16:48	22:09:00–22:26:24	945	$2.6 \times 10^{-15}$	0.23	
P	20 July	Not seen		945	—	0.23	Recorded but not played back. Signal likely too weak.
Q1	20 July	20:13:52	20:03:36–20:30:36	945	$1.1 \times 10^{-15}$	1.26	Two wavelengths alternate.
R	21 July	Not seen	05:34:03–05:44:43	678	$3.0 \times 10^{-15}$	5.3	Alternate samples played back. Signal too weak, or missed.
S	21 July	Not seen	15:21:00–15:59:25	945	—	0.23	Event shifted out of observed period.

\*Converted to equivalent UTC time for Earth-based observers.

†Time span is for data returned to Earth.

‡Signal maximum accounts for noise variance.

indicates rapid cooling, as the peak of the blackbody radiation shifted to longer wavelengths. This behavior is consistent with the brevity of the detection at 292 nm by the Galileo Ultraviolet Spectrometer (UVS) experiment for impact G (12) and the brief signal at 559 nm measured by the SSI for impact W (10).

An initial high temperature and small solid angle were also suggested for the G impact by the ratio of the Galileo UVS 292-nm flux to the PPR 945-nm flux during the rise to maximum signal (12). Behavior of the Near-Infrared Mapping Spectrometer (NIMS) spectra obtained seconds later for impact G are consistent with an expanding, cooling blackbody source with an initial temperature above 5000 K, going down to 450 K in just over 1 min (13). The atmospheric pressure levels implied from the NIMS methane-band data, when extrapolated backward to the time of the PPR peak, are near 200 mbar, well below where a meteor flash would be found.

If the first few seconds of the PPR flashes are from the meteor phase, the impacts should resemble large terrestrial meteor events; ablation by either terrestrial N<sub>2</sub> or Jovian H<sub>2</sub> would produce a hot vaporized layer of impactor material. Terrestrial meteors display a rich spectrum of metallic lines corresponding to excitation tempera-

tures in the range of several thousand kelvin (14). Most of these lines are in the blue region, with only weak continuum in the red and infrared (15). Consequently, we expect that the meteor phase would have been dim at the PPR-detected wavelengths, and at those used by the SSI camera (16).

It also seems unlikely that the intensity of the meteor phase would have so nicely merged into that of the subsequent fireball. The light curve shapes are similar for four events of differing magnitude (Fig. 5). The only indication of a separation is the aforementioned slope change, which could indicate termination of the trail or disappearance below clouds. However, it could also arise from development of a new opacity source within a cooling fireball.

The PPR measurements, together with those of the other Galileo experiments, imply a continuous impact radiation event, with no clear temporal distinction between an impacting meteor flash and subsequent fireball. That continuity is suggestive of the three-dimensional modeling of the impacts by Crawford *et al.* (4), who imply that the meteor entry above the level of obscuring clouds would be followed by immediate expansion of the upper portion of the entry channel into a hot, "line charge" fireball, aided perhaps by subsequent explosion of material from further down the channel. In

this comparison, the sharp initial rise of the PPR data may correspond to the fast passage of the fragment through the visible part of the atmosphere. The rise would be caused by a growing solid angle of the entry tube and the increasing conversion of the fragment's kinetic energy into heat. The abrupt cessation of the intensity rise is ascribed to either the bolide passing below a cloud layer or to final breakup of the body. The following part of the PPR curve, arising from a prompt fireball phenomenon, is simply the contribution of two competing terms: a cooling Planck emission and a growing solid angle, as in Eq. 1. The balance of these terms produces the flat part of the curve at 945 nm, and the downward acceleration of the signal indicates dominance of the cooling factor.

It is not necessary, in spite of the above arguments, to conclude from the Crawford *et al.* model prediction (4) that PPR detected the meteor phase emission. Comparison of PPR data to terrestrial telescopic data leads one away from that conclusion. Sensitive near-infrared (~2 μm) light curves of several impacts from various observatories typically show two low-amplitude events before the main infrared brightening (17–20). One interpretation of these three events is that they arose, respectively, from (i) the bolide, (ii) the plume emerging over the horizon, and (iii) the thermalization of the kinetic energy of the particles upon re-entry into the upper atmosphere.

The prospect that the initial bolide could be seen from Earth, either directly at the highest altitudes or from light refracted around the limb, is intriguing. A comparison of the timing of these events with Galileo observations is very instructive. For the G impact, the Anglo-Australian Telescope spectrometer (21) observed a faint pointlike source on the limb at 7:32:58, 39 s ahead of the PPR time. The first observation of the H impact by Calar Alto was 13 s before the PPR signal. For the L impact, both Calar Alto (17) and Pic-du-Midi (18) measured the first of these small "precursor" signals 13 to 16 s ahead of the PPR detection (Table 1). These comparisons are all consistent with the initial precursor flashes being faint signals observable from Earth several hundred kilometers above the point where the following PPR signal originates near a level of several millibars, based on the 200-mbar level implied by extrapolation of the NIMS G data and a vertical motion of  $2 \text{ s} \times 60 \text{ km s}^{-1} \times \cos(45^\circ)$ . They are also consistent with the initial PPR signal rise being part of the bolide phase, making the transition to the fireball phase. A similar argument can be made by comparing the timing of the initial SSI K data with the precursor observed at Okayama (20). For the G event, this interpretation implies that the sensitive Anglo-Australian Telescope detection (21) corre-

**Fig. 4.** Fluxes at 945 and 678 nm for impact Q1. The two polarization channels were averaged together for each wavelength, and periodic noise in one 678-nm channel was removed (see Fig. 2). The relative amplitude of these signals indicates a high temperature for the flash.

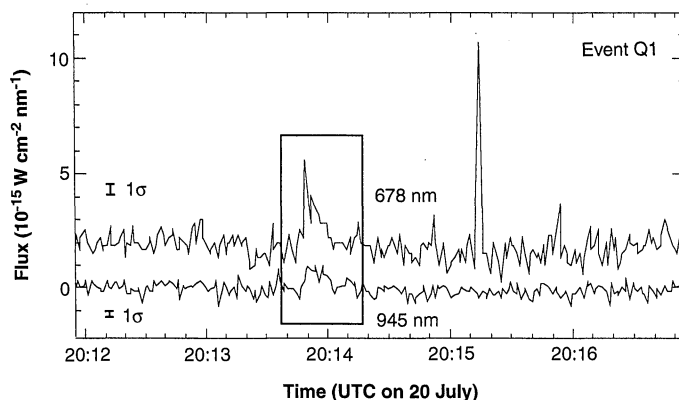
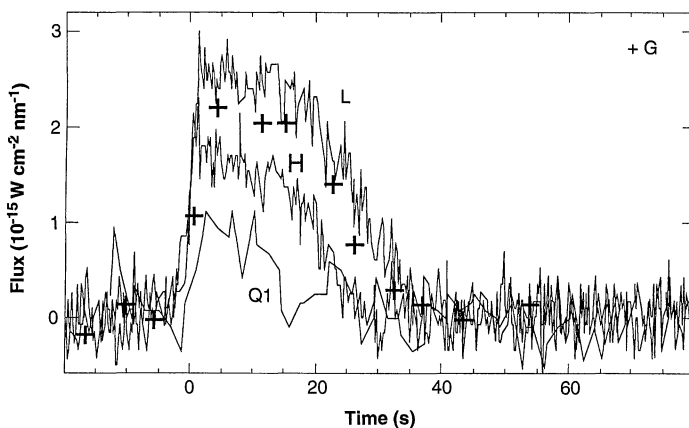


**Fig. 5.** Fluxes at 945 nm for the impacts G, H, L, and Q1. Data for G are shown as + symbols.



sponds to bolide emission at very high altitudes. It also implies that the 888-nm filter exposure made by the Hubble Space Telescope (HST) Wide Field Planetary Camera between 7:33:15 and 7:33:45 (22) detected the bolide phase. The HST integrated brightness was much less than that measured by the PPR at nearly the same wavelength within the same time frame, implying that most of the radiation detected by the PPR originated below the HST-observed limb (23). Obviously, the most complete picture of the first few seconds of the impact events will arise from detailed comparisons among the PPR and other Galileo observations and a large suite of terrestrial measurements at these and later times, together with models of the impact phenomenon.

We can readily determine an upper limit to the flux reflected from the closest Galilean satellite, Io, for the initial flash. The peak flux density for fragment L observed at a distance of 1.6 astronomical units (AU) by the PPR at 945 nm wavelength was  $2.7 \times 10^{-15} \text{ W cm}^{-2} \text{ nm}^{-1}$  (Fig. 5). Scaling that value to Io's distance from Jupiter's atmosphere ( $3.52 \times 10^5 \text{ km}$ ), we get  $1.26 \times 10^{-9} \text{ W cm}^{-2} \text{ nm}^{-1}$ , assuming isotropic emission from the impact point. Dividing this by the solar flux density at Jupiter at 945 nm ( $3.03 \times 10^{-6} \text{ W cm}^{-2} \text{ nm}^{-1}$ ) (24), we obtain  $4.15 \times 10^{-4}$ . This maximum brightening that might be expected for Io, 0.04% of Io's illuminated flux, would be difficult to detect and is consistent with the apparent lack of such reflected impact "flashes."

Much of the energy deposition may be hidden from view for deeper penetrating fragments, making mass estimation difficult or impossible. However, we can state a relative brightness on the basis of the 945-nm data. Using the peak signal values, we find that L, G, H, and Q1 had relative brightnesses of 2.4:2.1:1.6:1.0. The HST observations of the impact sites (22) provide a qualitative hierarchy in which the G, K, and L impact sites had the highest associated energy because of their large ejecta, central dark region more than 10,000 km in diameter, and multiple impact waves. The H impact site had a central dark region between 4000 and 8000 km in size, medium ejecta, and a single impact wave, and Q1 had a central dark region less than 3000 km with no ejecta and no observed impact wave. These are consistent with the ordering in energy that can be established with the PPR (and other Galileo) measurements. Further Earth-based measurements of comparative phenomena, such as amount of  $\text{NH}_3$  gas uplifted, column abundance of particulates generated, or amplitude of temperature perturbation, can provide significant additional constraints on the incoming fragment energy. On the other hand, pre-impact HST observations of the individual

cometary fragments gave relative brightnesses (25) for L, G, H, and Q1, of 1.00, 1.33, 0.80, and 1.40, respectively. These relative figures are in disagreement with our ordering and imply that a significant component of the observed comet brightness was contributed by particles that did not contribute substantially to the kinetic energy of the incoming fragment.

## REFERENCES AND NOTES

1. E. Russell *et al.*, *Space Sci. Rev.* **60**, 531 (1992).
2. Brief, bright emission from a small area was expected for the meteor flash as the comet fragments passed through the atmosphere. With the comet moving at  $60 \text{ km s}^{-1}$ , its passage through the atmosphere could have been short enough that the detectable signal was lost during rotation between filters. Radiation passes through a Wollaston prism in the PPR to separate orthogonal polarization components, which are sensed by separate detectors. These simultaneous measurements afforded an enhanced ability to confirm the reality of detections because the signal for a real event would appear in both channels, in contrast to random noise or spikes produced by cosmic rays hitting the silicon diode detector; the impact-induced radiation was unlikely to be polarized.
3. Predictions of impact conditions were made by several groups, including M. Boslough, D. A. Crawford, T. G. Trucano, A. C. Robinson, *Eos* **75**, 305 (1994); K. Zahnle and M.-M. Mac Low, *Icarus* **108**, 1 (1994); T. Takata, T. J. Ahrens, J. D. O'Keefe, G. S. Orton, *ibid.* **109**, 3 (1994).
4. D. A. Crawford, M. Boslough, T. G. Trucano, A. C. Robinson, *Shock Waves* **4**, 47 (1994).
5. The pointing stability of the Galileo scan platform permits targeting within the PPR field of view, and the viewing can be held to within about 1 mrad for long periods. Thus, it was practical to point at Jupiter and stare with the PPR for the duration desired. The observed signal levels and their constancy imply that steady pointing at Jupiter was achieved for the desired observing period.
6. The Galileo main antenna failed to open properly in 1992, leaving the spacecraft with diminished communications capacity. It was therefore necessary to plan for extended playback (about 6 months) of SL9 data acquired on the tape recorder for most of the remote sensing observations. However, another mechanism was available for instruments with low data rates such as the PPR [216 bits per second (bps)]. The PPR data were captured in the flight computer's memory and then read out with existing memory verification procedures. With 44 kilobytes of memory available, about 41 min of PPR data were stored in one sequence. At a nominal downlink rate of 10 bps, these data were sent to the Earth in about 12 hours. Having this early delivery of data from some of the impacts was intended to facilitate determination of relative timing of the impacts and thus enhance the ability to read out from the tape recorder selected data from other experiments, in the event that no Earth-based data were available to establish impact times.
7. Because the spacecraft scan platform, holding all of the co-aligned remote sensing instruments, has a small random pointing error, it was necessary to scan repetitively across Jupiter to ensure measuring it with the narrow slits of the spectrometers (UVS and NIMS). For observations of C, G, and R, designed for those instruments, the PPR data therefore consist of several on-Jupiter samples obtained for each scan period of 5.3 s at 945 nm. With telemetry time constraints allowing only alternating scans to be returned for the R impact, the PPR on-Jupiter samples for each 10.6-s interval at 678 nm show nothing above the normal levels associated with Jupiter. The same telemetry constraints precluded playback of the C data. Imaging sequences for events D, E, K, N, and W were done in data collection modes that prevented useful simultaneous PPR measurements.
8. We suspect that the fragment B impact was covered but was too small to be detected. Data recorded for P were considered unlikely to be useful, given reports from ground-based observers and the HST. Fragment S may have been detectable but apparently impacted before the start of our fixed observation window.
9. There was an unidentified spike in the Q1 data about 1.5 min after the principal event (Fig. 2). Although the principal event was seen in all four channels, this spike appeared only in the two 678-nm channels, and those amplitudes differed by more than a factor of 2. Although the amplitudes are well above noise levels, the brevity of the signature and its dissimilar amplitudes suggest this may have been a cosmic ray event affecting the two independent but physically adjacent detectors. No other event of this kind was seen in the entire SL9 data set.
10. For K, the Galileo camera shutter was held open as Jupiter was slewed across the field, providing a time-resolved trace of the flash brightness. For impact W, separate images of Jupiter were made each 2.3 s. C. R. Chapman *et al.*, *Geophys. Res. Lett.*, **22**, 1561 (1995).
11. The color temperature derived from the ratio of the 678- to 945-nm signal for event Q1,  $3.8 \pm 1.0$ , is highly sensitive to the absolute radiometric calibration of the PPR at these wavelengths. Although in-flight observations of Sirius confirmed the preflight calibration factor to within 5% at 410 nm, we have some doubt about the 945-nm calibration because the signals for Jupiter itself were about half of predicted levels. Until we can establish a reliable in-flight calibration for 678 and 945 nm, the estimated color temperature should be considered preliminary and subject to significant uncertainty. The nominal uncertainty of the ratio is consistent with color temperatures between 9,500 and 60,000 K.
12. C. W. Hord *et al.*, *Geophys. Res. Lett.* **22**, 1565 (1995).
13. R. W. Carlson *et al.*, *ibid.*, p. 1557.
14. For example, J. Borovicka [in *Meteoroids and Their Parent Bodies* (Astronomy Institute of the Slovak Academy of Science, Bratislava, Slovakia 1993)] derives an excitation temperature of 4000 K for a large terrestrial fireball. Analysis of meteoric production of heat and light was summarized by E. Öpik [in *Physics of Meteor Flight in the Atmosphere* (Interscience, New York, 1958)].
15. For example, P. M. Millman, in *Solid Particles in the Solar System*, I. Halliday and B. McIntosh, Eds. (Reidel, Dordrecht, Netherlands, 1980), pp. 121-128. Whereas terrestrial atmospheric emissions by N and O are weak in the visible region and contribute little to meteor spectra, the Paschen and Balmer lines of H should appear in jovian meteor spectra. Comets scatter sunlight in bands because of molecular radicals; near the PPR flight locations, J. R. Johnson, U. Fink, and S. M. Larson [*Icarus* **60**, 351 (1984)] show an  $\text{NH}_2$  feature in the region near 678 and a CN feature near 945 nm. Within 0.2 AU of the sun, atomic lines appear [G. W. Preston, *Astrophys. J.* **147**, 718 (1967)]. Postimpact spectroscopic observations of Jupiter [M. Roos-Serote *et al.*, *Geophys. Res. Lett.* **22**, 1621 (1995)] show a Li transition near 678 nm within a few minutes after each impact that could also be present in the initial flash.
16. This suggests that the meteor flashes would have been best detected in the blue and that if the PPR flashes contained radiation from the bolide, we poorly sampled the true luminosity of that phase.
17. D. P. Hamilton *et al.*, *Geophys. Res. Lett.*, in press.
18. P. Drossart *et al.*, *Bull. Am. Astron. Soc.* **26**, 1574 (1994).
19. J. R. Graham, I. de Pater, J. G. Jernigan, M. C. Liu, M. E. Brown, *Science* **267**, 1320 (1995); P. D. Nicholson *et al.*, *Geophys. Res. Lett.* **22**, 1613 (1995).
20. J. Watanabe *et al.*, *Publ. Astron. Soc. Jpn.* **47**, L21 (1995).
21. V. Meadows *et al.*, *Bull. Am. Astron. Soc.* **26**, 1588 (1994).
22. H. B. Hammel *et al.*, *Science* **267**, 1288 (1995).
23. The integrated interpretation of these events arose in a discussion among C. Chapman, P. Nicholson, and

- T.Z.M. based on comparison of Galileo PPR and SSI data with the Calar Alto and Pic-du-Midi observations of impacts H and L by Hamilton *et al.* (17) and Drossart *et al.* (18).
24. J. C. Arvesen, R. N. Griffin Jr., B. D. Pearson Jr., *Appl. Opt.* **8**, 2215 (1969).
25. H. A. Weaver *et al.*, *Science* **267**, 1282 (1995).
26. This research was carried out by the Jet Propulsion

Laboratory, California Institute of Technology, under a contract with the National Aeronautics and Space Administration. We acknowledge support from the Galileo Project. The impact timing predictions of P. Chodas and D. Yeomans were essential to the timing of the data acquisition.

2 December 1994; accepted 3 May 1995

## Outburst of Jupiter's Synchrotron Radiation After the Impact of Comet Shoemaker-Levy 9

Imke de Pater,\* C. Heiles, M. Wong, R. J. Maddalena, M. K. Bird, O. Funke, J. Neidhoefer, R. M. Price, M. Kesteven, M. Calabretta, M. J. Klein, S. Gulkis, S. J. Bolton, R. S. Foster, S. Sukumar, R. G. Strom, R. S. LePoole, T. Spoelstra, M. Robison, R. W. Hunstead, D. Campbell-Wilson, T. Ye, G. Dulk, Y. Leblanc, P. Galopecau, E. Gerard, A. Lecacheux

Jupiter's nonthermal microwave emission, as measured by a global network of 11 radio telescopes, increased dramatically during the Shoemaker-Levy 9 impacts. The increase was wavelength-dependent, varying from ~10 percent at 70 to 90 centimeters to ~45 percent at 6 and 36 centimeters. The radio spectrum hardened (flattened toward shorter wavelengths) considerably during the week of impacts and continued to harden afterward. After the week of cometary impacts, the flux density began to subside at all wavelengths and was still declining 3 months later. Very Large Array and Australia Telescope images of the brightness distribution showed the enhancement to be localized in longitude and concentrated near the magnetic equator. The evidence therefore suggests that the increase in flux density was caused by a change in the resident particle population, for example, through an energization or spatial redistribution of the emitting particles.

A worldwide network of radio telescopes was organized to observe Jupiter's flux density at microwave frequencies before, during, and after comet Shoemaker-Levy 9 (SL9) collided with the planet in July 1994.

I. de Pater, C. Heiles, M. Wong, Astronomy Department, University of California, Berkeley, CA 94720, USA.  
 R. J. Maddalena, National Radio Astronomy Observatory, Green Bank, WV 24944, USA.  
 M. K. Bird and O. Funke, Universität Bonn, 53121 Bonn, Germany.  
 J. Neidhoefer, Max-Planck-Institut für Radioastronomie, 53121 Bonn, Germany.  
 R. M. Price, M. Kesteven, M. Calabretta, Commonwealth Scientific and Industrial Research Organization, Epping, New South Wales 2121, Australia.  
 M. J. Klein, S. Gulkis, S. J. Bolton, Jet Propulsion Laboratory, Pasadena, CA 91109, USA.  
 R. S. Foster, Naval Research Laboratory, Code 7210, Washington, DC 20375, USA.  
 S. Sukumar, Dominion Radio Astrophysical Observatory, National Research Council, Penticton, British Columbia V2A 6K3, Canada.  
 R. G. Strom and T. Spoelstra, Netherlands Foundation for Research in Astronomy, Post Office Box 2, 7990 AA Dwingeloo, Netherlands.  
 R. S. LePoole, Leiden University, Post Office Box 9513, 2300 RA Leiden, Netherlands.  
 M. Robison, New Mexico Institute of Mining and Technology, Socorro, NM 87801, USA.  
 R. W. Hunstead, D. Campbell-Wilson, T. Ye, School of Physics, University of Sydney, New South Wales 2006, Australia.  
 G. Dulk, Astrophysical, Planetary, and Atmospheric Sciences, Boulder, CO 80309, USA.  
 Y. Leblanc, P. Galopecau, E. Gerard, A. Lecacheux, Observatoire de Paris, 92195 Meudon, France.

\*To whom correspondence should be addressed.

Our goal was to monitor Jupiter's microwave emission and to search for changes in the synchrotron radiation emitted by relativistic electrons (~1 to 300 MeV) trapped in Jupiter's inner magnetosphere.

The mechanism that produces the planet's steady synchrotron radiation is well understood, and the observed radiation characteristics were used in the early 1960s to derive Jupiter's magnetic field configuration and electron distributions (1). Jupiter's radio emission has been monitored continuously since the early 1970s at 13 cm (2). The flux density varies smoothly between ~3.5 and 5 Jy (1 jansky =  $10^{-26}$  W m<sup>-2</sup> Hz<sup>-1</sup>), over time scales of years. Although short-term time variability (days) in the flux density has been reported more than once (1), it has never been confirmed (3). During a jovian rotation, the flux density displays a sinusoidal variation in amplitude, commonly referred to as the "beaming curve" (Fig. 1). The peak-to-peak amplitude in the beaming curve is ~15%. The variation with jovian rotation of all radiation characteristics (in particular, the polarized components) implied a misalignment between the magnetic and rotational axes of ~10° and a confinement of most radiating electrons to the planet's magnetic equator (1).

It is usually assumed that electrons, on

average, diffuse inward in Jupiter's magnetosphere while the first adiabatic invariant is conserved. Hence, the particles gain energy in the diffusion process, and they lose it by synchrotron radiation. As the electrons move through the magnetosphere, they interact with solid material such as moonlets and dust, electromagnetic waves, and neutral and charged particles. All interactions usually result either in a loss of the electron or in a reduction in its energy (4).

Predictions before the event had concentrated on the interaction of the radiating electrons with cometary dust (5, 6). It was suggested that the radio emission would decrease as a result of energy degradation by cometary dust. This decrease would be most apparent at low frequencies. The highlight of the radio observations instead was a dramatic increase in the radio flux density during the 6 days of cometary bombardment. The increase in radio brightness was monotonic at a roughly constant rate during the week of impacts. Data taken during a 3-month period after the week of cometary impacts showed a steady decline in the radio flux density; by the end of October 1994, equilibrium had not yet been reached at the short wavelengths.

We observed Jupiter's radio emission between June and October 1994, with 11 different radio telescopes (single dishes and arrays of telescopes) (Table 1). We restricted our attention to total flux densities obtained at wavelengths between 6 and 90 cm (7). We calibrated all data against 3C286, either directly, or indirectly by means of a nearby secondary calibrator source (8). Although we also searched for burstlike emission (time scales varying from microseconds to seconds), no obvious activity or "radio bursts" could be associated with the times of impact events.

With the single dish telescopes, we determined the total flux density *S* of the planet either by scanning the planet in one (Nançay) or two (orthogonal) directions (Green Bank, Effelsberg, and Parkes) or by doing on-off scans (DSN and NRL) (see Table 1 for telescope abbreviations). Because the spatial extent of Jupiter's radio

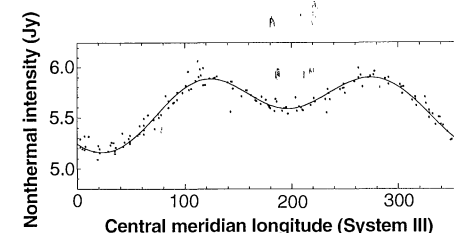


Fig. 1. A preimpact beaming curve (wavelength, 20 cm) of Jupiter's synchrotron radiation. The data were taken with the 140-foot NRAO telescope at Green Bank. Superposed is a best fit line after Eq. 1.